Supporting Information

Highly efficient visible-light driven photocatalysts: A case on zinc stannate based nanocrystal assemblies

Cai-Hong Liu,[1] *Robert Röder,*[2] *Lichun Zhang,*[1] *Zheng Ren,*[1] *Haiyan Chen,*[3] *Zhonghua Zhang,*[1] *Carsten Ronning,*[2] *and Pu-Xian Gao,*[1,] *

[1]Department of Materials Science and Engineering & Institute of Materials Science, University of Connecticut, Storrs, Connecticut 06269-3136, USA, [2]Friedrich-Schiller-Universität Jena, Institut für Festkörperphysik, Max-Wien-Platz 1, D-07743 Jena, Germany, [3]Mineral Physics Institute, Stony Brook University, Stony Brook, New York, 11794, USA

* Corresponding author E-mail: puxian.gao@ims.uconn.edu

Material evolution in thermal engineering of zinc hydroxylstannate nanocubes

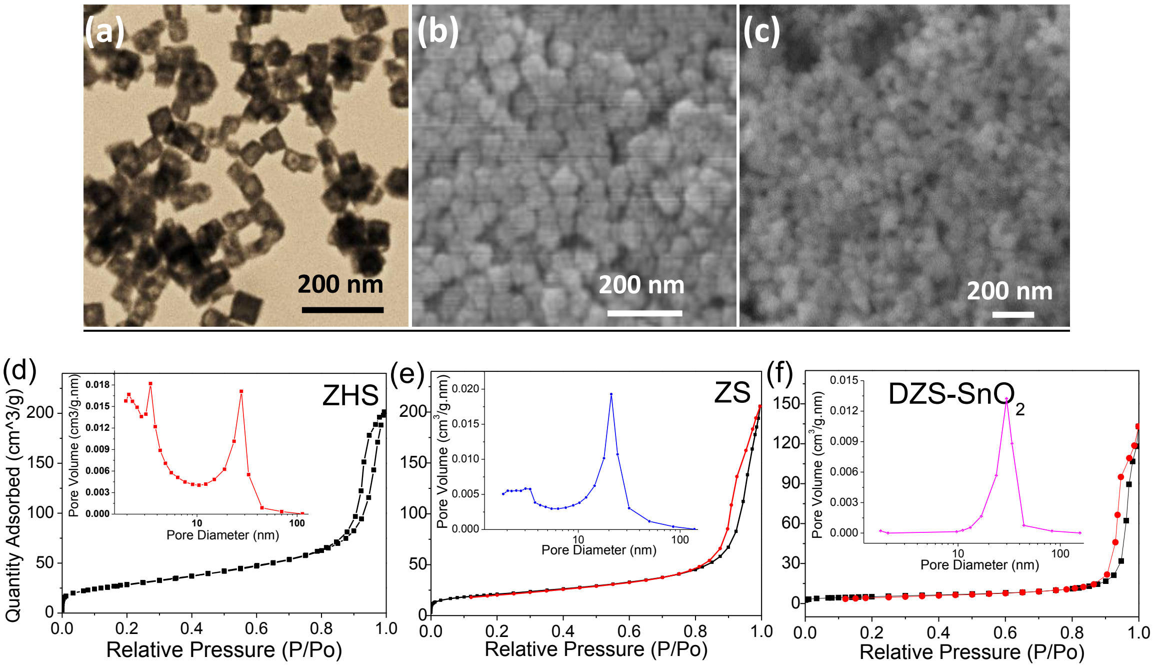

Figure S1. TEM and SEM images of the thermal treated products: ZS (a-b) and DZS-SnO_2 (c) nanoparticles. (d-f), nitrogen adsorption–desorption isotherms of zinc stannates nanostructures. Insets in (d-f): pore size distributions.

Table S1. Physico-chemical parameters of zinc stannates nanoparticles.

Nanoparticles	$ZnSn(OH)_6$	$ZnSnO_3$	Zn_2SnO_4-SnO_2
BET surface area /m².g^{-1}	104.1	75.5	18.0
Inner Pore size /nm	3.9±0.5	3.0±0.5	/
Particle size /nm	37±8	37±8	35±20

The characterization of their specific surface area and pore evolution after thermal treatment shows quite consistent results with HRTEM observations. The precursor ZHS has a very high specific surface area (104 m².g^{-1}), while amorphous ZS (75.5 m².g^{-1}) kept most of it due to maintenance of the porous structure; whereas DZS-SnO_2 (18 m².g^{-1}) showed a solid crystal structure hence lost most surface area of its precursor. The pore evolution after thermal treatment also can be traced from the pore distribution curves of the precursor in comparison with the two thermal products. A clear bimodal pore distribution of the plot of the precursor ZHS can be observed, which indicates N_2 adsorption at the inner pore (first peak below 10 nm) and the surface of the nanocubes (second peak, pore larger than 10 nm). The first peak decreased in ZS implying that the annealing partly destroys inner pores. While, the first pore peak disappeared and the second peak showed a little shift to a larger size in DZS-SnO_2, which can be easily understood based on the TEM observation results.

UV-vis absorption of P25 TiO_2 nanopowders

For comparison purpose, UV-vis absorption spectra were collected for solution suspension of P25 TiO_2 nanopowders using UV-vis spectrometer (Perkin Elmer 900). The typical spectrum in Figure S2 below illustrated the significant UV absorption with a certain degree of absorption in the visible range between 400 and 650 nm, which may be due to the diffusive scattering effect. The low catalytic degradation rate constant in the visible range light illumination further reflected the P25's low activity under visible light.

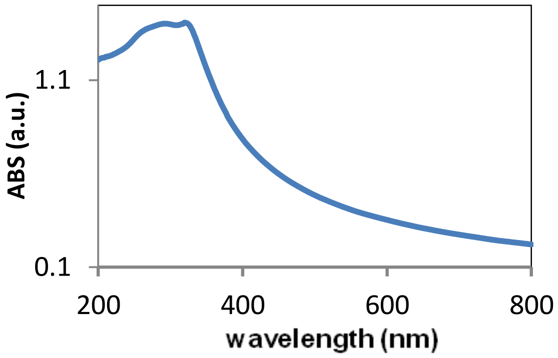

Figure S2. A typical UV-vis absorption spectrum of P25 TiO_2 nanoparticle suspension.

Photocatalytic mechanism

Based on the radical measurement experimental results, the photocatalytic process at the surface of zinc stannate nanoparticles has been proposed here. That is, electron-hole pairs are generated when zinc stannate are irradiated with UV-light. If not recombined, the electrons or holes can migrate to the surface and react with small molecules surrounding the particles, such as water, oxygen, and organic molecules. Then hydroxyl radical can form at the holes sites due to its highly reactive oxidation potential. Meanwhile, superoxide radicals can be created by electrons reacting with dissolved oxygen driven by a highly reactive reduction potential. The superoxide radicals may react with ions in solution and then ·OH also can be generated in this way. All these free radicals, which are highly reactive can attack organic molecules and hence degrade them. The process continues so that organic molecules can be totally mineralized to CO_2, H_2O and inorganic anions. The above proposed degradation routes can be shown in the following equations:

$$Zn_xSnO_y + h\nu \rightarrow e^- + h^+ \tag{1}$$

$$h^+ + H_2O \rightarrow H^+ + HO\cdot \tag{2}$$

$$e^- + O_2 \rightarrow O_2^-\cdot \tag{3}$$

$$O_2^-\cdot + e^- + 2H^+ \rightarrow H_2O_2 \tag{4}$$

$$e^- + H_2O_2 \rightarrow OH^- + OH\cdot \tag{5}$$

$$OH\cdot / O_2^-\cdot + RB \rightarrow \text{intermediates} \tag{6}$$

DZS-SnO_2 nanocrystal assemblies obtained after annealing with different ramping rate

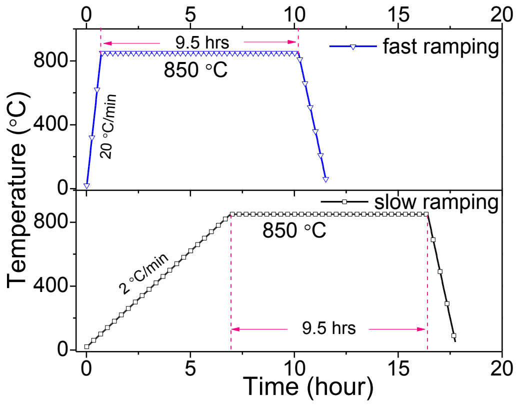

Figure S3. Temperature profiles for the fast and slow ramping to 850 °C.

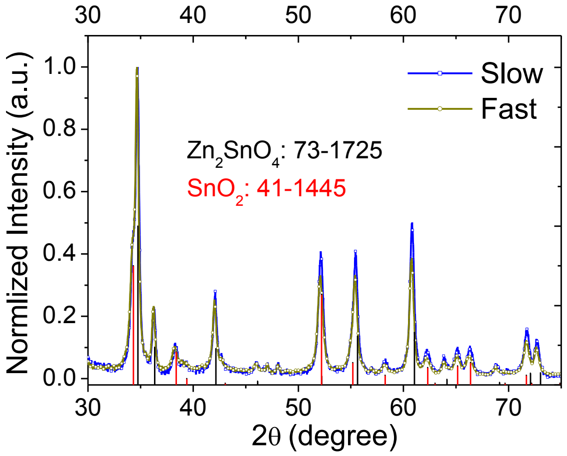

Figure S4. XRD spectra for DZS-SnO_2 slow and fast sample. JCPDS 73-1725 and JCPDS 41-1455 were shown for identifying spinel DZS and rutile SnO_2.

Based on the XRD data analysis (as shown in Figure S5), the crystallite size for DZS and SnO_2 can be calculated (three peaks for each were used). The average values of crystallite size of SnO_2 and DZS in slow-ramp are ~14.2 nm and ~22.8 nm, respectively. While, both SnO_2 and DZS in fast-ramp composite have much smaller crystallite size, which are 15.0 nm and 10.7 nm, respectively (The data were summarized in Table S2). Similar results on crystallite size have also been obtained from HRTEM observation.

Table S2. Crystallite sizes obtained from XRD calculation and TEM image simulation.

Charac. Samples	XRD		HRTEM	
	fast	slow	fast	slow
SnO_2	10.7± 3.0 nm	14.2± 3.0 nm	5-20 nm	10-25 nm
Zn_2SnO_4	15.0± 3.0 nm	22.8± 7.0 nm	10-25 nm	15-35 nm

Heterojunction induced photocatalytic performance enhancement

Synthesis of DZS nanoparticles. The spinel DZS nanoparticles were synthesized via a simple hydrothermal method, in which $ZnAc_2$ solution was added into $SnCl_4$ and hydrazine hydrate ($N_2H_4\cdot H_2O$) solutions as precursors in autoclave. Then, the precursor mixture solution was sealed and heated to 180 °C for 15 hours. The obtained white precipitate was collected and rinsed with DI water. SnO_2 nanoparticles were directly purchased from Alfa Aesar. Before mixing, the two substances were annealed at 850 °C for 9 hour with a ramping rate of 2 $°C.min^{-1}$ respectively. After thermal annealing, the nanomaterials were characterized by

XRD, SEM, TEM, and BET surface area tests. Typically, both spinel DZS and rutile SnO_2 have diameter smaller than 100 nm with irregular morphology. Their physical mixture has a specific surface area of 27.7 $m^2.g^{-1}$, much higher than those of fast-ramp (18 $m^2.g^{-1}$) and slow-ramp DZS-SnO_2 (15 $m^2.g^{-1}$) hetero-phase nanocrystals.

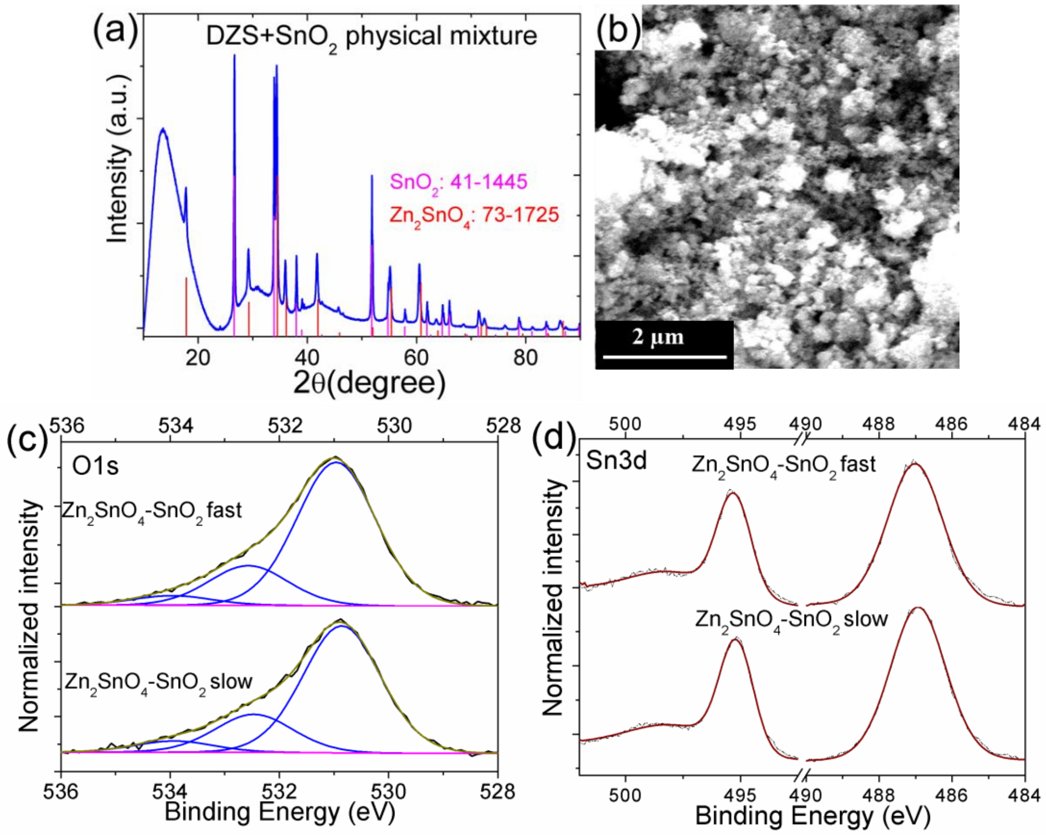

Figure S5. (a) XRD pattern and (b) SEM image of DZS-SnO_2 physical mixture. (c) O 1s and (d) Sn 3d XPS spectra of DZS-SnO_2 obtained via fast- and slow-ramping annealing.

Table S3. Peak positions of O 1s, Zn 2p, and Sn 3d in XPS spectra of DZS-SnO_2 obtained via fast- and slow-ramping annealing.

BE /eV **Samples**	**O1s**			**Zn 2p**		**Sn 3d**	
				2p 3/2	2p 1/2	3d 5/2	3d 3/2
DZS-SnO_2 fast	531.0	532.6	534.0	1024.9	1048.1	487.0	495.4
DZS-SnO_2 slow	530.9	532.5	534.0	1024.7	1047.9	487.0	495.3